Optik 125 (2014) 2633–2637

Contents lists available at ScienceDirect

Optik

journal homepage: www.elsevier.de/ijleo

Design of adaptive spatial filter at uniform standard for automatic analysis of digital holographic microscopy

Jiawen Weng[a], Hai Li[a], Zibang Zhang[b], Jingang Zhong[b,*]

[a] College of Science, South China Agricultural University, Guangzhou 510642, China
[b] Institute of Optoelectronic Engineering, Jinan University, Guangzhou 510632, China

ARTICLE INFO

Article history:
Received 3 June 2013
Accepted 2 November 2013

(090.1995) Digital holography
(070.6110) Spatial filtering
(120.5050) Phase measurement

ABSTRACT

The spatial filtering method is a useful technique for the dynamic and automatic analysis in digital holographic microscopy. It has been shown that the proper selection of the spatial filter would improve the quality of the reconstructed image. However different results would be obtained by employing the spatial filter with different parameter threshold decided at different standard. This paper, according to the histogram analysis of the distribution of the +1 term spectrum of each hologram, gropes for the uniform standard for the decision of the threshold of the adaptive filter. It helps the adaptive spatial filtering method to be more advantageous for the dynamic and automatic analysis.

© 2013 Elsevier GmbH. All rights reserved.

1. Introduction

Digital holographic microscopy is applied to the analysis of the micro-object because of the significant advantages, real time dynamic analysis [1–6], especially for the living cell image measurement [7,8]. For the digital holography, the digital holograms are recorded, and numerical methods are subsequently applied to reconstruct the image. How to suppress the dc term, conjugate term, noises, and parasitic interferences is very important in the numerical reconstruction process [9,10]. There are some methods, such as phase-shifting techniques [11–13] with the request of multiple digital holograms, and parallel phase-shifting digital holography [14–16] with the poor spatial resolution. For the analysis of the off-axis Fresnel hologram, the well-known Fresnel diffraction integral method [17] and the angular spectrum method [18] are employed. Here a very effective and versatile method, spatial filtering [19], is carried out to suppress the dc term and conjugate term, where the spatial filter plays the most important role. However, the distribution of the +1 term spectrum varies with different object to be measured. It means that, there is not a deterministic function for the description of the distribution of the +1 term spectrum. Therefore, it brings difficulties to define a precise spatial filter because of the non-regular boundary of the +1 term spectrum. In general, band pass filter, such as circular filter [20] and rectangular filter [21], are employed. For achieving precise analysis, manual spatial filters [22] are proposed to obtain the proper filter for different object at expense of consuming plenty of time for the dynamic analysis. Therefore, how to find out the distribution of the +1 term spectrum precisely and automatically is a very important and challenging work for the spatial filtering.

Filtering the +1 term spectrum in the frequency domain can be considered as the image segmentation [23] during the digital image processing. Thresholding algorithm [24] basing on the histogram analysis is one of the popular algorithms. According to the histogram analysis of the spectrum of each hologram, we find that, although the frequencies of the boundary of the +1 term spectrum in the frequency domain would be different, the corresponding intensities are basically the same. Therefore, we can employ the histogram analysis for the digital image of the power spectrum of the hologram to specify the intensity of different frequencies, and separate the +1 term spectrum by gray level thresholding. Weng and Zhong design an automatic spatial filter employing the thresholding, and discuss the main factor limiting the quality of the reconstructed image for the dynamic analysis [25]. But the filter would vary with different parameter threshold, which is decided by the complementary cumulative distribution function (CCDF) of the histogram of the power spectrum of the hologram by experience. It means that different results would be obtained according to the spatial filters decided at different standard. Therefore, it is necessary to grope for a uniform standard to define a proper spatial filter. In this paper, according to the histogram analysis of the spectrum of each hologram, a numerical reconstruction technique employing an adaptive filter that can be decided automatically at the uniform standard is proposed. The numerical simulation and the experiments with an onion specimen and a gastric cancer cell specimen are demonstrated the feasibility and validity of the principle. The detailed steps and analysis are presented.

* Corresponding author.
E-mail address: tzjg@jnu.edu.cn (J. Zhong).

0030-4026/$ – see front matter © 2013 Elsevier GmbH. All rights reserved.
http://dx.doi.org/10.1016/j.ijleo.2013.11.035

2. Spatial filtering in digital holography

The hologram is created by the interference, in off-axis geometry, between two coherent waves: on one side the wave of interest, called object wave $O(x, y)$, coming from the object, and on the other side a reference wave $R(x, y)$ being plane:

$$O(x, y) = o(x, y) \times \exp[jj(x, y)] \tag{1}$$

$$R(x, y) = R_0 \times \exp\left[j2\pi \frac{\sin\theta}{\lambda} x\right] \tag{2}$$

where (x, y) are the coordinates of the hologram plane; $o(x, y)$ and R_0 are the amplitude of the object and the reference waves; $\phi(x, y)$ is the phase of the object wave; λ is the wavelength; θ is the angle between the propagation direction of the object, and the reference waves on the x direction. The intensity of the hologram $I(x, y)$ can be written as:

$$I(x, y) = R \times R^* + O \times O^* + O \times R^* + O^* \times R \tag{3}$$

The first and the second terms form the zero-order term, namely the dc term. The third and the fourth terms are the virtual and the real image terms respectively. Employing the Fourier transform, the spectrum of the hologram at the hologram plane $z = 0$ is obtained as:

$$\begin{aligned} A(\xi, \eta; 0) &= \Im\{R \times R^* + O \times O^* + O \times R^* + O^* \times R\} \\ &= A_1(\xi, \eta; 0) + A_2(\xi, \eta; 0) + A_3(\xi, \eta; 0) + A_4(\xi, \eta; 0) \end{aligned} \tag{4}$$

Here $\Im\{\}$ denotes the Fourier transform, and (ξ, η) are the spatial frequencies of (x, y). $A_1(\xi, \eta; 0)$ and $A_2(\xi, \eta; 0)$ represent the zero term of the spectrum, $A_3(\xi, \eta; 0)$ is the +1 term or the virtual image term, and $A_4(\xi, \eta; 0)$ is the -1 term or the real image term. When employing a proper spatial filter, the spectrum $A_3(\xi, \eta; 0)$ can be obtained. Shift $A_3(\xi, \eta; 0)$ to the center of the frequency domain. According to the angular theory, the spectrum of the reconstructed wave at the plane of distance z perpendicular to the propagation axis from the hologram plane, i.e., $A_3(\xi, \eta; z)$, can be calculated from $A_3(\xi, \eta; 0)$ as:

$$A_3(\xi, \eta; z) = A_3(\xi, \eta; 0) \times \exp\left[j\frac{2\pi z}{\lambda}\sqrt{1 - (\lambda\xi)^2 - (\lambda\eta)^2}\right] \tag{5}$$

Subsequently the reconstructed wave can be obtained by taking the inverse Fourier transform as:

$$U(x', y'; z) = \Im^{-1}\{A_3(\xi, \eta; z)\} \tag{6}$$

where $\Im^{-1}\{\}$ denotes the inverse Fourier transform and (x', y') are the coordinates of the image plane.

During the processing, the most important is to define a proper spatial filter according to the distribution of the +1 term spectrum. However, there is not a deterministic function for the description of the boundary of the +1 term spectrum, which varies with different object to be measure. In order to find out the boundary, the numerical analysis of the distribution of the +1 term spectrum of each hologram should be preformed.

3. Experimental method and results

The apparatus depicted analogous to a Mach–Zehnder interferometer as shown in Fig. 1. A He–Ne laser beam (wavelength of 632.8 nm) is separated into two beams by a beam splitter BS1. One beam serves as a reference wave, and another beam illuminates the biological specimen. A microscope objective MO1 (16×, 0.3NA) collects the object wave transmitted by the specimen and produces a magnified image of the specimen at a distance behind the CCD camera. Another MO2 (16×, 0.3NA) is placed in the reference arm, so that the two beams have matching wave front curvatures. The beam splitter BS2 placed in front of a CCD camera (MINTRON 22K9HC, 795 × 596 pixels, 8.33 × 8.33 μm² per pixel) combines the two beams, and the holograms are recorded by the CCD camera with 8-bit gray scale output. A slight angle is introduced between the object and the reference beams by tilting the beam splitter BS2 for the off-axis holography.

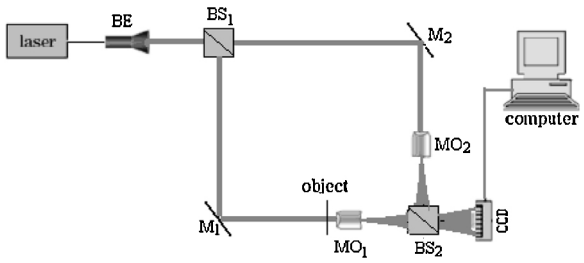

Fig. 1. Apparatus for digital holography experiment.

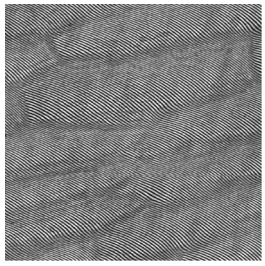

Fig. 2. The hologram with an onion specimen of size 512 × 512 pixels.

3.1. Analysis of the +1 term spectrum

Fig. 2 shows the hologram with an onion specimen of size 512 × 512 pixels. First, the logarithm operation is performed for the power spectrum to balance the energy of the +1 term spectrum for avoiding the high spectrum of the object being lost during the numerical analysis. Fig. 3 shows the rough scope of the distribution of the +1 term spectrum with the logarithm operation and normalization by an elliptic binary filter centered at (ξ_c, η_c) with major and minor axis of $(0.9\xi_c, 0.9\eta_c)$, where $(\xi_c, \eta_c) \in (0, 0.5) \times (-0.5, 0.5)$ corresponding to the center of the +1 term spectrum. Here the intensity of the frequency (ξ_c, η_c) is 1 corresponding to the gray value 255, and the intensity of the suppressed frequencies is 0 corresponding to the gray value 0. We can see that, although the frequencies of the boundary of the distribution of the +1 term spectrum in the frequency domain would be different, the corresponding intensities are basically the same. Therefore, we can employ the histogram analysis for the digital image of the power

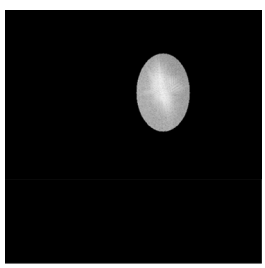

Fig. 3. The distribution of the +1 term spectrum of the hologram with an onion specimen.

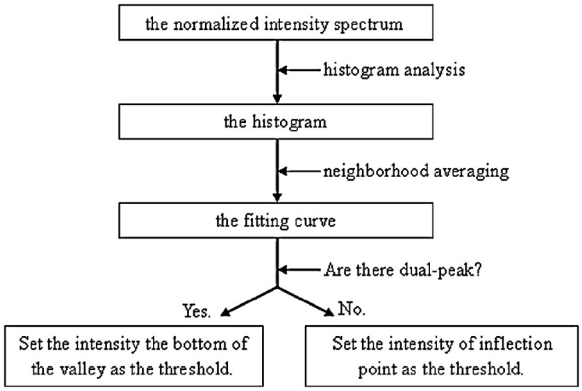

Fig. 4. The analysis flow chart.

spectrum of the hologram to find out the gray value, which corresponds to the frequencies of the boundary of the +1 term spectrum.

3.2. Histogram analysis for determining the threshold

Fig. 4 shows the analysis flow chart. First, the histogram analysis with 256 gray bins for Fig. 3 is employed to specify the intensity of different frequencies. Fig. 5(a) shows the counts corresponding to different gray values, where the count of gray value 0 being missed. By the analysis of Fig. 5(a), we can find that the peak point corresponds to the intensity of the background spectrum within the binary filter, and the counts have a marked drop after the peak. In general, the threshold can be selected at the bottom of the valley between the peaks [26–28]. However, the valleys do not exist in Fig. 5(a). But we still can find the inflection point at the shoulder of the peak, which corresponds to the concavities. And with the intensity increasing, the counts rise slowly with the appearance of +1 term spectrum. Therefore, the gray value of the first inflection point after the peak corresponds to the intensity of the boundary of the +1 term spectrum. By employing numerical fitting analysis method, we can determine the intensity of the boundary of the +1 term spectrum by the gray value of the inflection point. And the threshold can be determined according to the intensity of this inflection point.

For the determination of the inflection point, the neighborhood averaging method is employed to smooth the data to obtain a fitting curve. Here, the neighborhood averaging process is performed 10 times iterative computations with the template 1/5[1,1,1,1,1]. The fitting curve is the black line as shown in Fig. 5(a), whose mean squared error is 7.56. Fig. 5(b) and (c) show the 1st and 2nd derivative of the fitting curve. The peak point appears at the intensity 176/256, where the value of the 1st derivative being zero. And the first inflection point of the fitting curve after the peak point appears at the intensity 188/256, where the value of the 2nd derivative being zero. Therefore, the threshold thr. of the adaptive filter is set to be 188/256 for the analysis of the hologram with the onion specimen as shown in Fig. 2. On the other hand, from Fig. 5(a), the fitting curve is much similar to the Gaussian function. It means that the Gaussian function is one of the appropriate functions for the curve fitting. When employing a

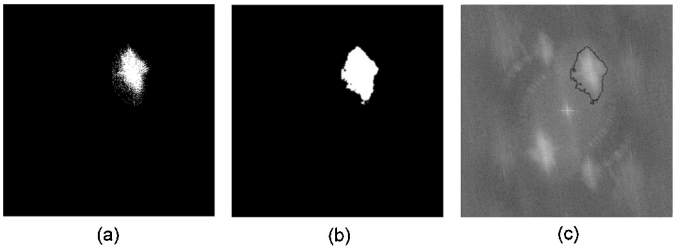

Fig. 6. The adaptive spatial filter for the hologram with an onion specimen. (a) The threshold filtering, (b) the averaging filtering and, (c) the spectrum with the black line window representing the adaptive spatial filter.

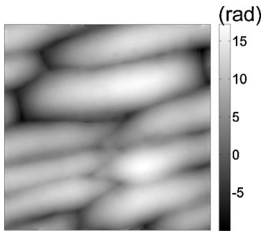

Fig. 7. The reconstructed phase image from the hologram with an onion specimen.

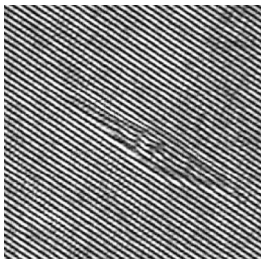

Fig. 8. The hologram with a gastric cancer cell specimen of size 256 × 256 pixels.

sum of Gaussian function $f(x) = \sum_{k=1}^{2} A_k \exp\left[-(x - x_k)^2/2\sigma_k^2\right]$ [29] for the curve fitting, the threshold thr. is 193/256.

3.3. Determination of adaptive spatial filter

Suppose that $S_{\text{rect}}(\xi, \eta)$ represents the intensity of the spectrum as shown in Fig. 3, there is:

$$S_{\text{thr}}(\xi, \eta) = \begin{cases} 1 & \text{where } S_{\text{rect}}(\xi, \eta) \geq \text{thr} \\ 0 & \text{where } S_{\text{rect}}(\xi, \eta) < \text{thr} \end{cases} \quad (7)$$

$S_{\text{thr}}(\xi, \eta)$ indicates the discrete distribution area of the +1 term spectrum as shown in Fig. 6(a). By applying the convolution operation to Fig. 6(a) with a mean filter $1/4\begin{bmatrix} 1 & 1 \\ 1 & 1 \end{bmatrix}$, the continuous distribution area of the +1 term spectrum can be obtained as shown in Fig. 6(b). Therefore, the adaptive filter can be determined according to the boundary of the +1 term spectrum. Fig. 6(c) shows the

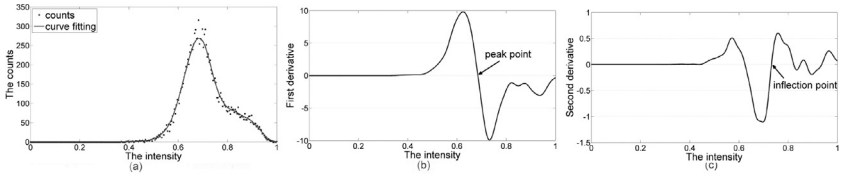

Fig. 5. (a) The histogram analysis for the hologram spectrum with an onion specimen and the fitting curve; (b) the 1st and, (c) the 2nd derivative of the fitting curve.

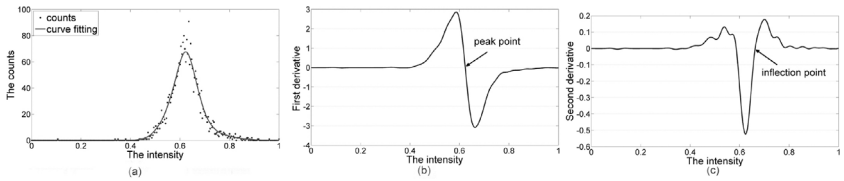

Fig. 9. (a) The histogram analysis for the hologram spectrum with a gastric cancer cell specimen and the fitting curve; (b) the 1st and, (c) the 2nd derivative of the fitting curve.

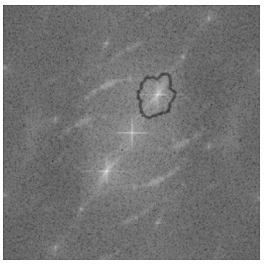

Fig. 10. The spectrum of the hologram with a gastric cancer cell specimen, where the black line window representing the adaptive spatial filter.

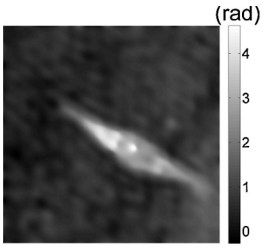

Fig. 11. The reconstructed phase image from the hologram with a gastric cancer cell specimen.

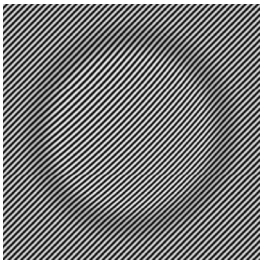

Fig. 12. The digital hologram generated by the computer.

spectrum of the hologram with the logarithm operation, where the black line representing the adaptive spatial filter. According to the angular theory, the reconstructed phase image can be obtained as shown in Fig. 7.

3.4. Analysis of hologram with gastric cancer cell specimen

The same analysis processing is performed for the hologram with the gastric cancer cell specimen of size 256×256 pixels, as shown in Fig. 8. When employing 256 gray bins for the histogram analysis, the threshold thr. is 170/256. Fig. 9(a) shows the counts at each intensity level, and the fitting curve whose mean squared error is 3.21. Fig. 9(b) and (c) show the 1st and 2nd derivative of the curve fitting. The peak point appears at the intensity 160/256. And the inflection point appears at the intensity 170/256, i.e., the value of the threshold thr. Fig. 10 shows the spectrum of the hologram with the logarithm operation, where the black line representing the adaptive spatial filter. Fig. 11 shows the reconstructed phase image. We can see that, the proposed method is fit for the analysis of different object in digital holography.

4. Discussion

A numerical simulation with a phase-contrast object of 256×256 pixels is presented to discuss the errors. The amplitude of the object is set to be one, and the phase distribution is calculated by the following function:

$$\phi(m,n)=\begin{cases}\dfrac{\sqrt{(m\text{-}128)^2+(n\text{-}128)^2}}{12} & \text{where } (m\text{-}128)^2+(n\text{-}128)^2 \le 96^2 \quad (m,n\in Z^+)\\ 0 & \text{others}\end{cases} \tag{8}$$

here (m,n) represents the position in pixel. Considering the biological specimens mainly generate the phase modulation being slowly varying, the aforementioned phase distribution is performed filtering with a circular averaging filter of radius 10 pixels. Fig. 12 shows the digital hologram generated by the computer. Fig. 13 shows the reconstructed phase image by the spatial filter decided at the uniform standard, and the reconstructed phase image by different thresholds with CCDF = 0.01 and 0.001 corresponding to the conventional method presented in Ref. [25]. As shown in Fig. 14, the absolute error is within 0.0267 rad by employing the proper filter decided at the uniform standard automatically. But the maximum absolute error would be about 0.3336 rad with an improper threshold.

The proposed method can be applied for the analysis of the spatial carrier-fringe signal, such as three-dimensional shape measurement. And for the application, it should be noted the following two points. First, when employing the spatial filtering method for

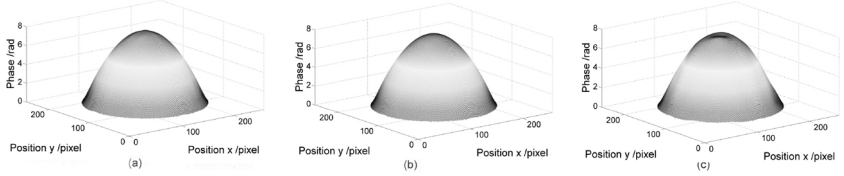

Fig. 13. (a) The reconstructed phase image by the spatial filter decided at the uniform standard, and by other spatial filters with different thresholds corresponding to CCDF to be, (b) 0.01, and (c) 0.001.

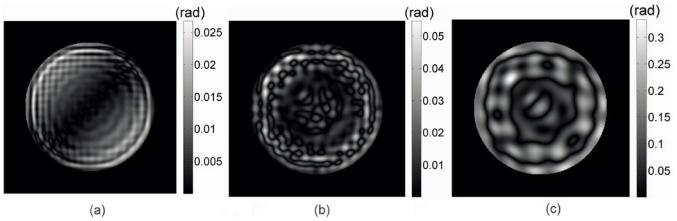

Fig. 14. The absolute errors by employing a proper filter (a) decided at the uniform standard and with thresholds corresponding to CCDF to be, (b) 0.01, and (c) 0.001.

analysis, the interesting spectrum should be band width and should not be overlapped by the other term spectrum. Second, when the energy of the interesting spectrum is much concentrative, more gray bins should be used for the histogram analysis to find out the inflection point precisely. For example here, for the analysis of the hologram with the gastric cancer cell specimen, when employing 512 gray bins for the histogram analysis, the threshold thr. is 338/512.

5. Conclusion

In this paper, by employing the histogram analysis of the digital image of the power spectrum of the hologram, a numerical reconstruction technique employing an adaptive filter that can be performed automatically at the uniform standard is proposed. It helps the spatial filtering method to be more advantageous for the dynamic and automatic analysis. According to the numerical analysis of the distribution of the +1 term spectrum of each hologram, the threshold is set to be equal to the intensity of the first inflection point of the fitting curve after the peak point. The detailed steps and analysis are presented by the experiment with an onion specimen and a gastric cancer cell specimen. The results demonstrate the feasibility and validity of the principle.

Acknowledgments

This research was supported by National Natural Science Foundation of China under the Grant Nos. 61077003 and 61307011, and Foundation for Distinguished Young Talents in Higher Education of Guangdong China under the Grant No. LYM10036.

References

[1] J. Kühn, T. Colomb, F. Montfort, F. Charrière, Y. Emery, E. Cuche, P. Marquet, C. Depeursinge, Real-time dual-wavelength digital holographic microscopy with a single hologram acquisition, Opt. Express 12 (2007) 7231–7242.
[2] T. Shimobaba, Y. Sato, J. Miura, M. Takenouchi, T. Ito, Real-time digital holographic microscopy using the graphic processing unit, Opt. Express 16 (2008) 11776–11781.
[3] B. Kemper, G. von Bally, Digital holographic microscopy for live cell applications and technical inspection, Appl. Opt. 47 (2008) A52–A61.
[4] P. Langehanenberg, B. Kemper, D. Dirksen, G. von Bally, Autofocusing in digital holographic phase contrast microscopy on pure phase objects for live cell imaging, Appl. Opt. 47 (2008) D176–D182.
[5] T. Shimobaba, N. Masuda, Y. Ichihashi, T. Ito, Real-time digital holographic microscopy observable in multi-view and multi-resolution, J. Opt. 12 (2010) 065402.
[6] A. Anand, V.K. Chhaniwal, B. Javidi, Real-time digital holographic microscopy for phase contrast 3D imaging of dynamic phenomena, IEEE/OSA J. Display Technol. 6 (2010) 500–505.
[7] P. Marquet, B. Rappaz, P.J. Magistretti, E. Cuche, Y. Emery, T. Colomb, C. Depeursinge, Digital holographic microscopy: a noninvasive contrast imaging technique allowing quantitative visualization of living cells with subwavelength axial accuracy, Opt. Lett. 30 (2005) 468–470.
[8] F. Charriere, B. Rappaz, J. Kuhn, T. Colomb, P. Marquetand, C. Depeursinge, Influence of shot noise on phase measurement accuracy in digital holographic microscopy, Opt. Express 15 (2007) 8818–8831.
[9] T. Kreis, Handbook of holographic interferometry, in: Digital Recording and Numerical Reconstruction of Wave Fields, Academic, 2005, pp. 105–108.
[10] Myung K. Kim, Suppression of DC and Twin-Image Terms in Digital Holographic Microscopy, Academic, 2011, pp. 85–93.
[11] Y. Takaki, H. Kawai, H. Ohzu, Hybrid holographic microscopy free of conjugate and zero-order images, Appl. Opt. 38 (1999) 4990–4996.
[12] Y.M. Zhang, Q.N. Lu, B.Z. Ge, Elimination of zero-order diffraction in digital off-axis holography, Opt. Commun. 240 (2004) 261–267.
[13] D. Carl, B. Kemper, G. Wernicke, G. von Bally, Parameter-optimized digital holographic microscope for high-resolution living-cell analysis, Appl. Opt. 43 (2004) 6536–6544.
[14] T. Kakue, R. Yonesaka, T. Tahara, Y. Awatsuji, K. Nishio, S. Ura, T. Kubota, O. Matoba, High-speed phase imaging by parallel phase-shifting digital holography, Opt. Lett. 36 (2011) 4131–4133.
[15] T. Kakue, S. Itoh, P. Xia, T. Tahara, Y. Awatsuji, K. Nishio, S. Ura, T. Kubota, O. Matoba, Single-shot femtosecond-pulsed phase-shifting digital holography, Opt. Express 20 (2012) 20286–20291.
[16] T. Tahara, R. Yonesaka, S. Yamamoto, T. Kakue, P. Xia, Y. Awatsuji, K. Nishio, S. Ura, T. Kubota, High-speed three-dimensional microscope for dynamically moving biological objects based on parallel phase-shifting digital holographic microscopy, IEEE J. Sel. Top. Quant. Elect. 18 (2012) 1387–1393.
[17] E. Cuche, P. Marquet, C. Depeursinge, Simultaneous amplitude-contrast and quantitative phase-contrast microscopy by numerical reconstruction of Fresnel off-holograms, Appl. Opt. 34 (1999) 6994–7001.
[18] L. Yu, M.K. Kim, Wavelength-scanning digital interference holography for tomographic three-dimensional imaging by use of the angular spectrum method, Opt. Lett. 30 (2005) 2092–2094.
[19] M.K. Kim, L. Yu, C.J. Mann, Interference techniques in digital holography, J. Opt. A 8 (2006) 518–523.
[20] E. Cuche, P. Marquet, C. Depeursinge, Spatial filtering for zero-order and twin-image elimination in digital off-axis holography, Appl. Opt. 39 (2000) 4070–4075.
[21] C. Mann, L. Yu, C.-M. Lo, M. Kim, High-resolution quantitative phase-contrast microscopy by digital holography, Opt. Express 13 (2005) 8693–8698.
[22] T. Colomb, J. Kühn, F. Charrière, C. Depeursinge, Total aberrations compensation in digital holographic microscopy with a reference conjugated hologram, Opt. Express 14 (2006) 4300–4306.
[23] R.C. Gonzalez, R.E. Woods, Digital Image Processing, 3rd ed., Addison-Wesley, 1992.
[24] M. Sezgin, Survey over image thresholding techniques and quantitative performance evaluation, J. Electron. Imaging 13 (2004) 146–165.
[25] Jiawen Weng, Zhong Jingang, Hu Cuiying, Automatic spatial filtering to obtain the virtual image term in digital holographic microscopy, Appl. Opt. 49 (2010) 189–195.
[26] A. Rosenfeld, P.D. Torre, Histogram concavity analysis as an aid in threshold selection, IEEE Trans. Syst. Man Cybern.-13 23 (1983) 1–235.
[27] C.A. Glasbey, An analysis of histogram-based thresholding algorithms, Graph. Model. Im. Proc. 55 (1993) 532–537.
[28] D.M. Tsai, A fast thresholding selection procedure for multimodal and unimodal histograms, Pattern Recogn. Lett. 16 (1995) 653–666.
[29] A. Goshtasby, W.D. O'Neill, Curve fitting by a sum of Gaussians, Graph. Model. Im. Proc. 56 (1994) 281–288.